

# CNN Based Early Vision Models for Color vision and Visual Illusions

*Ákos Zarándy<sup>+‡#</sup>, L. Orzó<sup>\*#</sup>, Edward Grawes<sup>‡</sup>, and Frank Werblin<sup>†</sup>*

<sup>\*</sup>Laboratory of Neurobiology, Department of Anatomy, Semmelweis Medical School (SOTE), Tüzoltó u. 58, Budapest, H-1014 email: orzo@ana1.sote.hu

<sup>#</sup>Neuromorphic Information Technology, Graduate Center, Kende u. 13. Budapest, H-1111

<sup>+</sup>Computer and Automation Institute of the Hungarian Academy of Science (SZTAKI), 11 Lágymányosi út, Budapest, H-1111, Hungary, email: zarándy@lutra.sztaki.hu, roska@lutra.sztaki.hu.

<sup>‡</sup>Nonlinear Electronics Laboratory of the University of California, Berkeley, CA 94720 USA, email: akos@fred.eecs.berkeley.edu, edwardg@ocf.berkeley.edu roska@fred.eecs.berkeley.edu, chua@fred.eecs.berkeley.edu

<sup>†</sup>Department of Molecular and Cell Biology, University of California at Berkeley email: werblin@mander.berkeley.edu

**ABSTRACT:** CNN models are introduced to analyze and explain the human early vision color perception and some of the visual illusions. CNN model of Horn's algorithm is shown, and a new lightness determination method is introduced. CNN models for the Zöllner, the Café Wall, the Poggendorf, the Brightness, and the Face-Vase illusion are also introduced.

## 1. Introduction

Cellular Neural Networks (CNNs) show strong resemblance with the biological visual systems. It is not surprising that several CNN models were produced for unraveling the processing some parts of the vertebrate visual pathway [7,9,12,13,14]. Most of these works was devoted to examine the early vision stages (retina) [7,9,12,14], and some of them for further parts of the visual pathway (LGN, cortex) [7,13]. The first CNN models of the color vision [5,8] reflected the basic neuromorphic models [11]. In this paper we apply this knowledge to prove the usefulness of these models in the understanding of color vision and in the explanation some of the visual illusions.

Determination of colors in a complex scene with electro-optical devices does not seem to be difficult. However, it is. It is almost as difficult as the measurement of flavors of a meal with electro-chemical devices. The reason is in both case, that these phenomena are based on the mainly unknown properties of the human perception. Land demonstrated in his famous experiment the ambiguousness of the human color perception [1,2]. He also introduced a model framework (retinex theory), which can describe the human color perception. Main component of this framework is the lightness determination, what he called "retinex computation". In the first part of the paper we show different lightness determination models. These CNN based neuromorphic models might form the basis of a real-time color measurement unit, which can

determine the object's color in arbitrary environments. This kind of measuring devices do not exist today, since the precise model of the human color perception is not achieved yet.

For the sake of better understanding of human visual information processing, it is necessary to be able to reproduce or at least qualitatively explain, not only the common mechanisms, but also some of the peculiar performance of the visual system also. CNN seems to be a natural framework for these experiments due to its special retinotopical structure. Within this framework, we can give bottom-up explanations for the majority of visual illusions. Relatively simple CNN structures can be given which are able to simulate the vertebrate visual information processing. These CNN structures are motivated by known inner representation of the visual inputs and their interactions. In the second part of this paper, we demonstrate that some of these inner representations can be responsible for some types of visual illusions. It is not fully understood what kind of interactions refine the different representations within the visual cortex. Building a more comprehensive model of the visual system can lead better image segmentation algorithms. With these experiment we prove that most of the visual illusion are generated at the early vision level and not in the cognitive level.

In this paper first, we refresh Land's experiment [1] in Section 2, then the retinex framework [1,2] is shown in Section 3. In Section 4, Horn's lightness determination algorithm [3] and its CNN model is introduced. Then, a new neuromorphic CNN based lightness determination model is offered in Section 5. Section 6 we quickly overview the previous studies on the CNN illusion models. Then, in Section 7 CNN based explanations of some well known visual illusions are introduced. Finally, in Section 8 we give the conclusion of our results.

## 2. Land's Experiments

In his famous experiments Land showed [1,2] that the received RGB triplet from a color object sometimes does not show definite correlation with the perceived natural color. He showed, that under different illumination conditions, the received triplets from the objects with totally different colors can be the same, however, human observer still can distinguish them.

In his experimental setup, there was a large laboratory display (he titled it as "Mondrian" after the great painter), utilizing about 100 colored papers. A paper of a given color appeared many times in different positions of the display, each time having different size and shape, and each time being surrounded by a different set of other colored papers. The Mondrian was illuminated by three independently controllable monochromatic light sources: with a long-wave, a middle-wave, and a short-wave. From now, we reserve the name of the colors for those situation, when a human observer reports the chromatic property of an object. In all other cases we will talk about bandwidths or bandwidth distributions. The bandwidth of the light sources were appropriate roughly to the three existing visual pigments. A telescopic photometer was placed next to the human observer. It received and measured the radiation from a very small area of the display. The area was much smaller, than a colored paper piece. The experimental setup can be seen in Figure 1.

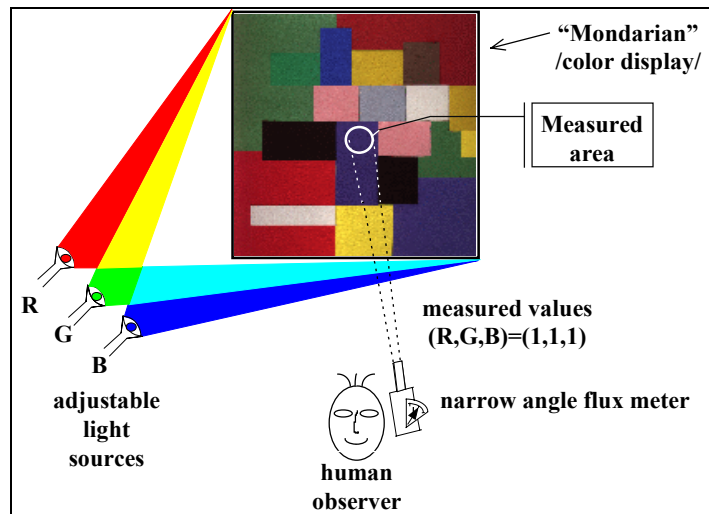


Figure 1. The experimental setup of Land's experiments.

Four different papers were chosen on the display: a yellow, a white, a green, and a blue one. The telescope was pointed first to the yellow paper. The short-wave and the middle-wave illuminators were switched off, and the whole Mondrian was illuminated with the long-wave light source. The illuminator was tuned until the meter read exactly "one" ( $0.1\text{W/Sr}^2/\text{m}^2$ ). The long-wave illuminator was turned off and then middle-wave illuminator was turned on. It was adjusted until the meter reads the same value as before. Finally, it was done for the third projector as well. This ensured, that the amounts of long-wave, middle-wave, and short-wave energy reaching the meter from that small patch are equal, when all the illumination sources are on. If a true color digital image would have been taken from this scene (with all the three illuminators on) the same RGB pixel value triplet (1,1,1) would describe the color of that particular location. In the forthcoming sections we will deal with these triplets.

When all the three illuminators were switched on, for a human observer the yellow paper looks yellow. Then, the attention was turned to the white paper, and exactly the same adjustment was done on the light sources. After turning all the illuminators on, one can expect, that the white paper will appear yellow, because the same radiation distribution is reflected from it as in the previous case. However, it appeared to be white! Then, the same was repeated with the green and the blue papers, and the green paper's color was reported as green, the blue was reported as blue.

In another experiment of him [1], he used the same experimental setup, and used the four different papers as well. First he focus the attention to the yellow paper and tuned the projectors till it reads one-one-one. Then asked the human observer to report the color of all the four selected papers. The observer perceived the yellow paper as yellow, the white one as white, the green one as green, and so the blue one as blue. He pointed the meter on the white paper and tuned the projectors again, till the meter read one-one-one. After switching on all the three light sources, the human observer reported the colors of all the papers correctly as well. Finally, he did the same experiment with the green and the blue papers, and the human observer still could report correctly the colors, against the fact that the illumination conditions were drastically changing during the experiments. This phenomenon is called *color constancy*.

### 3. The structure of Land's retinex model

Knowing Land's results one can ask: If the reflected wavelength composition do not, than what is responsible for the colors of an object? Physically, the *reflectance coefficient* is the only measurable illumination independent (but certainly wavelength dependent) constant. This property of an object is called lightness in a monochromatic environment. This fact seems to be responsible for the natural color of objects. The *reflectance coefficient* can be calculated using the following form:

$$R_{\lambda} = \frac{E_{R\lambda}}{E_{I\lambda}} \quad (1)$$

where:  $R_{\lambda}$  is the reflectance coefficient,  $E_{R\lambda}$  is the energy of the reflected radiation, and  $E_{I\lambda}$  is the energy of the illumination at a given wavelength ( $\lambda$ ). If  $R_L, R_M, R_S$ , (the reflectance coefficients in the long, middle, and short wave regions) are known, the color of an object is assumed to be known. Color scanners exactly do this. They use narrow bandwidth illumination sources with known energy, and measure the energy of the reflected light. The triplets they get in this way ( $R_L, R_M, R_S$ ) defines the colors.

Land proposed the retinex model which is a three channel model for color identification. Each channel deals with a certain bandwidth (Long, Middle, Short; LMS) without interaction. An estimated reflectance (or lightness) map of the scene is calculated in each channel. Figure 2 shows the structure of Land's retinex model. The incoming image is split to three individual monochromatic maps. In all channels the same retinex computation (lightness determination) is done.

As we saw in the previous section, the LMS triplets of the incoming intensity image do not define unequivocally the colors. Land stated in [1,2] that with appropriate retinex processing methods the LMS triplets of the processed image define the colors. The triplets can be visualized in the LMS space. When the triplets from the incoming image are displayed in this chart, the dots are shuffled and dots belonging to the same colors usually do not form separated groups. But when the triplets from the processed images are displayed, the dots corresponding to particular colors form groups, and the different color groups are clearly separated. We will see this kind of charts in Sections 5.

Land introduced some methods for retinex computations [1,2], but those are not very feasible from the biological aspect, and on the other hand those work well on those type of images which contain large unicolored areas separated by sharp edges. In the next sections we show two retinex (lightness) computational methods.

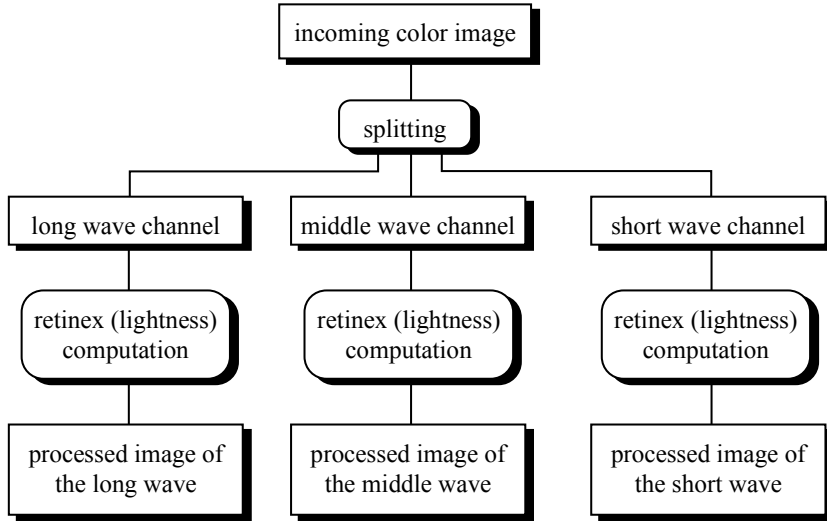


Figure 2. The structure of Land's tri-channel retinex model.

## 4. Horn's model for determining lightness

In this section as an introduction to the lightness determination method first we show Land's 1D continuous space method [3]. Then we show Horn's 2D method, and finally its CNN model is introduced.

### 4.1 Land's 1D continuous space method for determining lightness

Land invented a simple method for separating the image components in one dimension. (Recall that we would like to know  $R_\lambda$ , but we now only  $E_{I\lambda}R_\lambda$ .) First he took logarithms to convert the product of the illumination and the reflectance into sum:

$$E_{R\lambda} = E_{I\lambda}R_\lambda \quad \log E_{R\lambda} = \log E_{I\lambda} + \log R_\lambda \quad (2)$$

This is followed by differentiation. The derivative will be the sum of the derivatives of the two components. The edges will produce sharp pulses of area proportional to the intensity steps between the regions, while the spatial variation of illumination will produce only finite values everywhere. If the finite values are discarded with a thresholding, the derivatives of the lightness (reflectance map) remains. This can be restored by integration. Figure 3 shows the steps of the method.

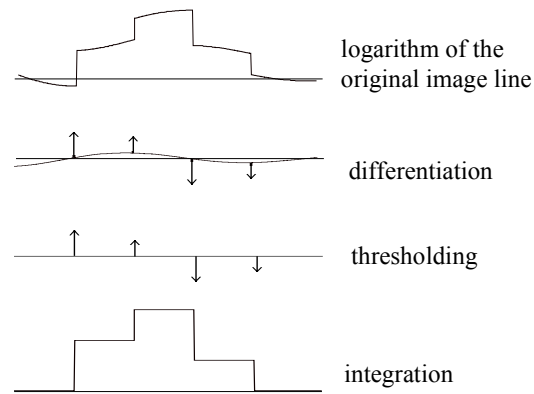


Figure 3. Processing steps in Land's 1D lightness determination method. The illumination on the original image changes slowly, and the edges of the areas causes the steps in the function. After the derivation, the steps became pulses (indicated with arrows). Then, the small components are discarded by a threshold operation. Finally, the lightness is calculated by integrating the pulses.

#### 4.2 Horn's 2D method for determining lightness

Horn generalized Land's 1D method [3]. He used hexagonal pixel representation of an image (2D signal). He replaced the differentiation operator with the Laplace operator. The Laplace operator was calculated with the following hexagonal convolution kernel:

$$\begin{array}{c}
 \begin{array}{cc}
 \text{hexagon} & \text{hexagon} \\
 -1/6 & -1/6 \\
 \text{hexagon} & \text{hexagon} \\
 -1/6 & 1 & -1/6 \\
 \text{hexagon} & \text{hexagon} \\
 -1/6 & -1/6
 \end{array} \\
 (3)
 \end{array}$$

The Laplace operator was followed by the thresholding. It was simple so far, but the inverse Laplace transformation is not a trivial operation. For a well defined hexagonal pixel array with well defined boundary conditions it can be done with matrix inversion. But while the original matrix (which calculated the Laplace) was a sparse matrix with 1s in the diagonal and -1/6 scattered around, the inverted matrix is not sparse any more [3]. This makes the direct matrix inversion method not very feasible in the retina, because there are mostly local interconnections, which can be described with a sparse matrix.

To overcome this problem, Horn introduced an iterative method for computing the inverse transformation [3]. This applies local interconnections between linear summing devices only. The schematic of his structure can be seen in Figure 4.

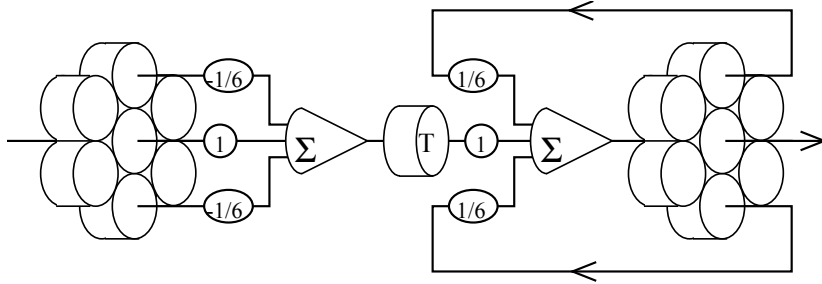


Figure 4. The schematic of Horn's model using summing and thresholding elements. The feedforward structure calculates the Laplace operator, while the feedback loop structure calculates the inverse Laplace operation. Note, that for the shake of clarity of the figure not all the feedback and feedforward interconnections are indicated.

The convolution kernel of the kernel loop is as follows:

$$\begin{array}{ccc}
 & 1/6 & 1/6 \\
 1/6 & 0 & 1/6 \\
 & 1/6 & 1/6
 \end{array} \quad (4)$$

### 4.3 The CNN implementation of Horn's model

If we analyze Horn's model (Figure 4) we find its structure to be similar to the CNN. The feedforward part can be implemented with a single **B** template, the threshold with a nonlinear element, and the feedback loop with an **A** template. Though Horn suggested the hexagonal arrangement, here we implement the model on a rectangular structure. The two layer CNN can be seen in Figure 5.

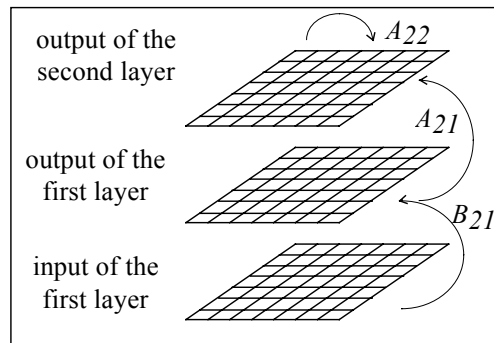
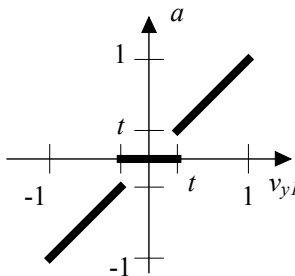


Figure 5. The proposed CNN structure for implementing Horn's model. The first and the second grid represents the input and the output of the first layer, while the third grid stands for the output of the second layer.

The templates are as follows:

$$B_{11} = \begin{bmatrix} -0.125 & -0.125 & -0.125 \\ -0.125 & 1 & -0.125 \\ -0.125 & -0.125 & -0.125 \end{bmatrix}, \quad A_{21} = \begin{bmatrix} 0 & 0 & 0 \\ 0 & a & 0 \\ 0 & 0 & 0 \end{bmatrix},$$

$$A_{22} = \begin{bmatrix} 0.125 & 0.125 & 0.125 \\ 0.125 & 1 & 0.125 \\ 0.125 & 0.125 & 0.125 \end{bmatrix}$$

(5)

$B_{11}$  calculates the Laplace operator, and transfers the result into the output of the first layer. The output of the first layer is connected to the second layer through nonlinear a function  $A_{21}$ . The inverse Laplace function is calculated on the second layer  $A_{22}$ . The central element of  $A_{22}$  is +1 for eliminating effect of the resistor in the CNN cell. (ide nem kell  $A_{22}(2,2)=1$ ! Latszik is a rekonstrukcion hogy nem pontos mert kicsit kiemelte a szineket... Persze nem igazan lenyeges a tartalom szempontjabol! ☺ ...)

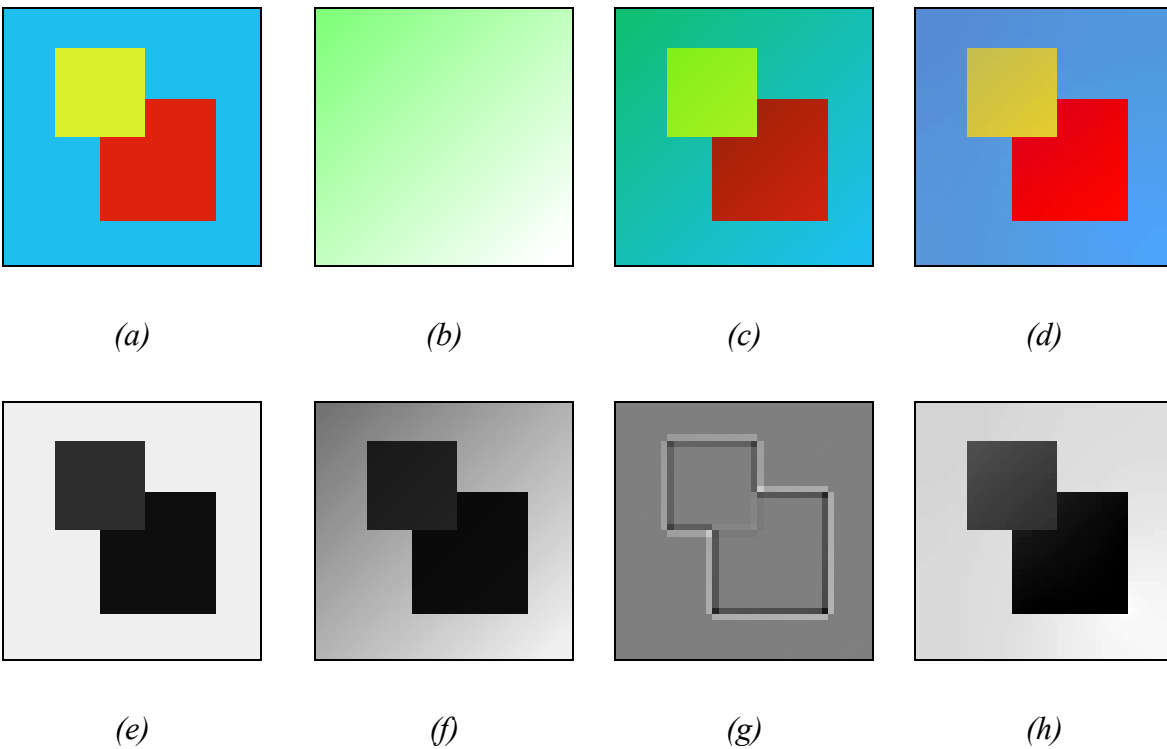


Figure 6. Example for Horn's lightness determination model. (a) is the original test image (before illumination) and (b) is the illumination pattern. (c) is the illuminated image, as the human observer perceives it. This is the input of the three channel retinex model. (d) is the result. It is clearly seen on (d), that the method restored the yellow square, which became green due to the chromatic illumination on (c). Figures (e)-(h) shows the processing steps in a single channel. (e) is the short monochromatic



*channel of the original image (before illumination). (f) is the illuminated image. (g) is the result of the Laplace operator. (h) is the final result.*

For illustrating the method, we show a simple example. In Figure 6a a color image given ( $R_\lambda$ ). It is illuminated with a light source. Figure 6b shows the chroma distribution of the illumination in space ( $E_{I\lambda}$ ). Figure 6c shows the illuminated image how a human observer would perceive ( $E_{I\lambda}R_\lambda$ ) it. This is the input of algorithm. It is split into three monochromatic channels. We applied the described CNN method on each channel, and combined the monochromatic maps again (Figure 6d). Due to the greenish illumination, the yellow square turned to greenish yellow (Figure 6c), but it is yellow again in the processed image (Figure 6d). Figure 6(e)-(h) shows the processing steps in a single channel.

## 5. A CNN based neuromorphic lightness determination method

The basis of the color vision is the calculation (or estimation) of the lightness (reflectance map) of the long, medium, and short wavelength sensitive channels. The lightness can be calculated by the division of the reflected light and the illumination (1). But for a human observer two problems arise. First of all, the human eye can perceive (*measure*) the energy of the reflected light ( $E_{R\lambda} = E_{I\lambda}R_\lambda$ ) only, but cannot perceive the energy of the illumination. (For measuring the illumination energy, the sensor should be located on the surface of the object!) The other problem is, that our neurons can be very good in the addition and subtraction of signals, but they cannot solve easily the division..

Our neuromorphic lightness computation model finds solution for both problems. The model estimates the overall illumination energy by large scale averaging of the visual scene. The lack of division can be overcome by using logarithmic input-output characteristics (like our photo-sensitive cones do), and then applying subtraction. The model contains three stages: the input layer with logarithmic characteristics, the illumination estimator, and the difference calculator. The operation of the model can be traced along in Figure 7.  $E_{I\lambda}R_\lambda$  is the incoming image.  $R_\lambda$  is the spatial reflectance map (lightness) distribution at the given wavelength.  $E_{I\lambda}$  is the energy of the illumination, which changes slowly in space. The sensory layer captures the images, and does a pixel-wise logarithmic transformation on them. The illumination estimator calculates the average in a large neighborhood. The spatial averaging of a 2D signal is denoted by a horizontal bar above the term.  $\log E_{I\lambda} \cong \overline{\log E_{I\lambda}}$ , because  $E_{I\lambda}$  changes slowly in space.

In the nature  $E_{I\lambda}$  usually changes slowly. But there are some important cases, when the chromatic distribution of the illumination changes rapidly. Consider a slide show. The human observer can see different colors on the screen, however, the screen is a large, flat, white object without any  $R_\lambda$  changes. How can it happen? What happens with the *Color constancy* in this situation? The rapid chromatic changes in the illumination cheat the eye, which is not prepared for them. It shows, that the color constancy is true only under certain circumstances. These circumstances are usual, and frequently occurs in natural environments. Our neuromorphic model deals only with those situations, when the color constancy is valid.

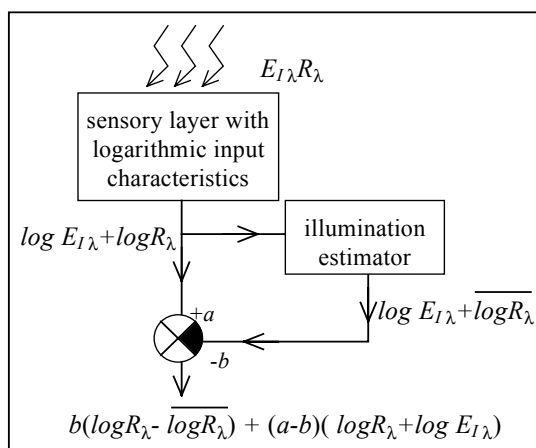


Figure 7. The flow-chart of the process in a single monochromatic channel.

At the end of the process, the weighted subtraction is calculated (Figure 7). Parameters  $a$  and  $b$  play very important role in the model. For example, if we choose  $a=b$ , then we can get rid of the  $E_{I\lambda}$  term, hence we can eliminate the disturbing effect of the illumination. But then, the first term will carry visual information only, which is not satisfactory. Consider the following example: someone is seated in a closed room with red walls. He or she cannot see anything else, just the red wall everywhere. In this case, the first term becomes zero, because the  $R_\lambda$  is constant in space, hence,  $\overline{\log R_\lambda} = \log R_\lambda$ , which results, that no information will be transferred towards the brain. However, the observer will see red color. So, it is better to choose  $a \neq b$ . If we choose  $a$  a bit greater than  $b$ , our model will separate the colors robustly. ( $a < b$  would lead to inversion, because with the increasing illumination the channel response would decrease.)

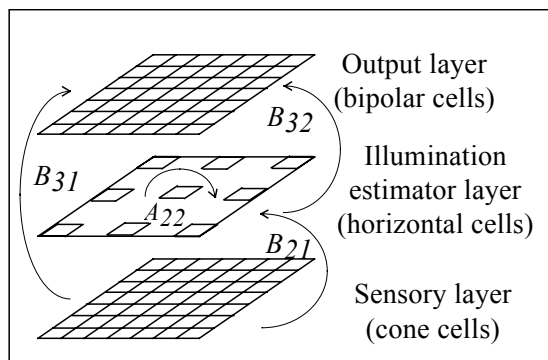


Figure 8. The CNN implementation of the proposed neuromorphic lightness determination method.

We implemented our lightness determination algorithm on a 3 layer CNN structure (Figure 8). The first layer is the sensory layer with logarithmic input characteristics. This represents the cone cell layer of the retina. The second layer which stands for the horizontal cells, is a low density layer. It calculates the spatial averaging. The third layer which corresponds to the bipolar cell layer of the retina calculates the subtraction. We used the following templates to implement the

process: (Minek kell ilyen nagy szomszedsag amikor ugy is feedback template, legfeljebb tovabb fut...? Ja ha tobb szin bemenet osszeget atlagolnad akkor talan lehetne meg javitani a dolgon...! A horizontalis sejt neha igy is csinalja, de ha nem is pont ilyen akkor sem csak a saját con-jainak a jelet csatolja vissza hanem egy nagy diverz populacio atlagat...igy latszik a szin mindenkepp stb. Ir is valami ilyet az egyik referee)

$$A_{22} = \begin{pmatrix} 0.012 & 0.012 & 0.012 & 0.012 & 0.012 & 0.012 & 0.012 \\ 0.012 & 0.023 & 0.023 & 0.023 & 0.023 & 0.023 & 0.012 \\ 0.012 & 0.023 & 0.029 & 0.029 & 0.029 & 0.023 & 0.012 \\ 0.012 & 0.023 & 0.029 & 0.056 & 0.029 & 0.023 & 0.012 \\ 0.012 & 0.023 & 0.029 & 0.029 & 0.029 & 0.023 & 0.012 \\ 0.012 & 0.023 & 0.023 & 0.023 & 0.023 & 0.023 & 0.012 \\ 0.012 & 0.012 & 0.012 & 0.012 & 0.012 & 0.012 & 0.012 \end{pmatrix}, \quad B_{32} = \begin{pmatrix} -0.1 & -0.2 & -0.1 \\ -0.2 & 0 & -0.2 \\ -0.1 & -0.2 & -0.1 \end{pmatrix}, \quad \begin{matrix} B_{31} = [1.4], \\ B_{21} = [0.056], \end{matrix} \quad (6)$$

We evaluated our model by reproducing Land’s second experiment. The input images were the same ‘Mondrian’ displays (Figure 1) under different illumination conditions. The illumination conditions are the same as it was previously described in Section 2. We picked up intensity value triplets from the input image from 4 different locations (yellow, white, green, and blue areas) under the four illumination conditions. The measured triplet values can be found in Table 1. Figure 9a shows the triplets in a 3D plot. As it can be seen, the points belonging to the same colors form completely overlapping sets.

	<b>Yellow</b>	<b>White</b>	<b>Green</b>	<b>Blue</b>
<b>Illumination 1</b>	(1; 1; 1)	(1.13; 1.33; 4.78)	(0.34; 0.64; 1.56)	(0.21; 0.27; 3.13)
<b>Illumination 2</b>	(0.87; 0.75; 0.21)	(1; 1; 1)	(0.3; 0.48; 0.33)	(0.19; 0.23; 0.66)
<b>Illumination 3</b>	(3.84; 1.54; 0.63)	(3.97; 2.06; 3.05)	(1; 1; 1)	(0.76; 0.48; 2.03)
<b>Illumination 4</b>	(4.56; 3.21; 0.31)	(5.21; 4.29; 1.5)	(1.17; 1.36; 1.16)	(1; 1; 1)

Table 1. Triplets received from 4 different locations of the image ( $E_{R\lambda} = E_{I\lambda} R_{\lambda}$ ) under different illumination conditions. Columns contain incoming triplets coming the same location of the ‘Mondrian’ under different illumination conditions.

After the images were processed, we picked up triplets from the same locations. The triplets can be found in Table 2. Figure 9b shows the 3D plot of the *processed triplets*. As it can be seen, the colors are robustly separated.

	Yellow	White	Green	Blue
<b>Illumination 1</b>	(1.32; 1.37; 1.03)	(1.34; 1.44; 1.55)	(1.08; 1.28; 1.22)	(0.84; 0.99; 1.4)
<b>Illumination 2</b>	(1.30; 1.36; 0.94)	(1.33; 1.42; 1.45)	(1.07; 1.27; 1.13)	(0.84; 0.96; 1.31)
<b>Illumination 3</b>	(1.38; 1.4; 1)	(1.4; 1.47; 1.52)	(1.14; 1.32; 1.2)	(0.91; 1.01; 1.38)
<b>Illumination 4</b>	(1.41; 1.44; 0.96)	(1.44; 1.52; 1.47)	(1.17; 1.36; 1.16)	(0.94; 1.05; 1.34)

Table 2. The processed triplets from the same locations.

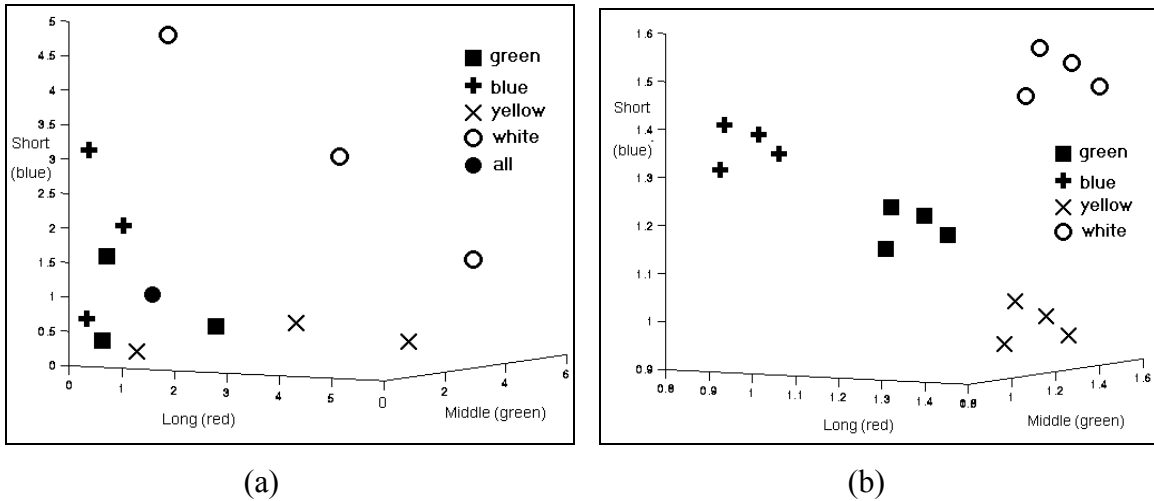


Figure 9. The 3D plot of the triplets from the input images (a), and the 3D plot of triplets from the processed images from the same location (b). While the colors are coded ambiguously on the raw image, they are well separated after the processing.

## 6. Previous studies on CNN based visual illusion models

The understanding and the reproduction of visual illusions were always a challenge for the information processing theorists [16, 17, 18, 19]. Cellular Neural Networks seem to be adequate as a conceptual framework for modeling these effects. However, there were only a few attempts to model different illusions within this paradigm [7,10]. There were preliminary works presented about modeling the well-known Müller-Lyer and Herring grid illusions (Figure 10a,b), in which the authors used modified CNN retina models. Later nice results arose about the CNN simulation of Kanizsa Illusory Contour and Angular Location Illusions (Figure 10c,d).

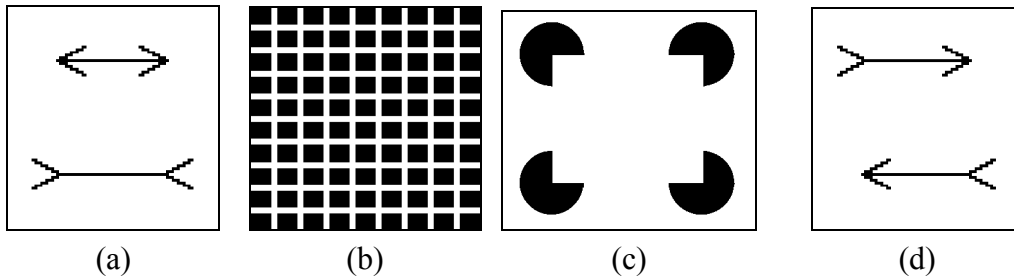


Figure 10. Some illusions, which were already modeled with CNN.

Here we assume that the vast majority of the visual illusions occur due to the alteration of the inner representation of the visual input by the interaction of the visual system components. The reproduction of different types of illusions do not necessarily require distinct representations. Here we will show, that a large group of illusions can be explained by akin mechanisms, that is by the same representation of the input or the same interaction between similar representations.

## 7. CNN models of some well-known Visual illusions

### 7.1 Zöllner illusion

Figure 11 shows the Zöllner illusion. The lines are parallel, but the crossing lines cause them to appear to diverge.

To understand this phenomenon, one has to carefully examine what kind of effects are caused by the crossing lines. The most important primary effect is that small black patches appear at the acute angles, and no changes happen at the obtuse angles. This can even be seen by the naked eye (Figure 11a.). The small black patches are exaggerated in Figure 11b. We consider, that in a higher level of our visual system the crossing lines are erased, but the patches still remain at the end of the line pieces (Figure 11c.).

The patches at the end of the line pieces fool the brain when it computes their orientation. It can be imagined in the following way: the ends of the line pieces seem to be moved towards the patches which cause them to appear being rotated. Figure 11d shows an exaggerated draw, which illustrates what we see.

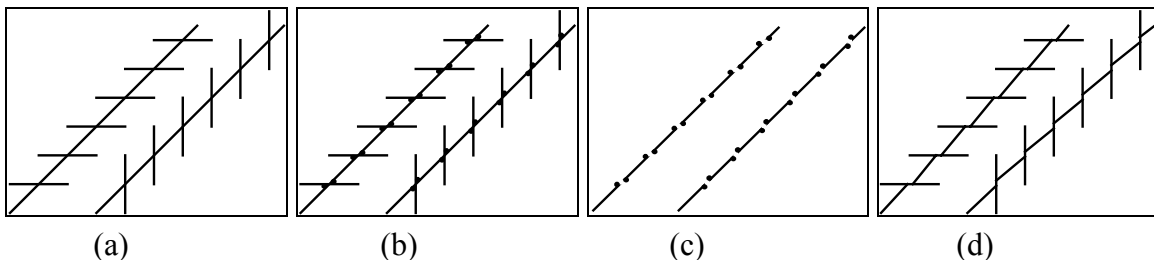


Figure 11. The original Zöllner illusion (a). The magnified patches at the acute angles (b). The cut line pieces with the patches (c). The magnified distortion caused by the crossing lines (d).

We created structural-strategy model for this illusion. The appearance of the patches is derived from the structure of the retina, while the rotation effect is explained by the behavior of the orientation selective cells in the cortex [11].

The appearance of the patches is the result of a blurring which can be found in the retina [11]. This can be modeled by the following feed forward template:

$$A=[0], \quad B=\begin{bmatrix} 0.023 & 0.023 & 0.023 & 0.023 & 0.023 \\ 0.023 & 0.053 & 0.055 & 0.053 & 0.023 \\ 0.023 & 0.055 & 0.2 & 0.055 & 0.023 \\ 0.023 & 0.053 & 0.055 & 0.053 & 0.023 \\ 0.023 & 0.023 & 0.023 & 0.023 & 0.023 \end{bmatrix}, \quad I=0 \quad (7)$$

(The input can be seen in Figure 12a, and the output can be seen in Figure 12b.)

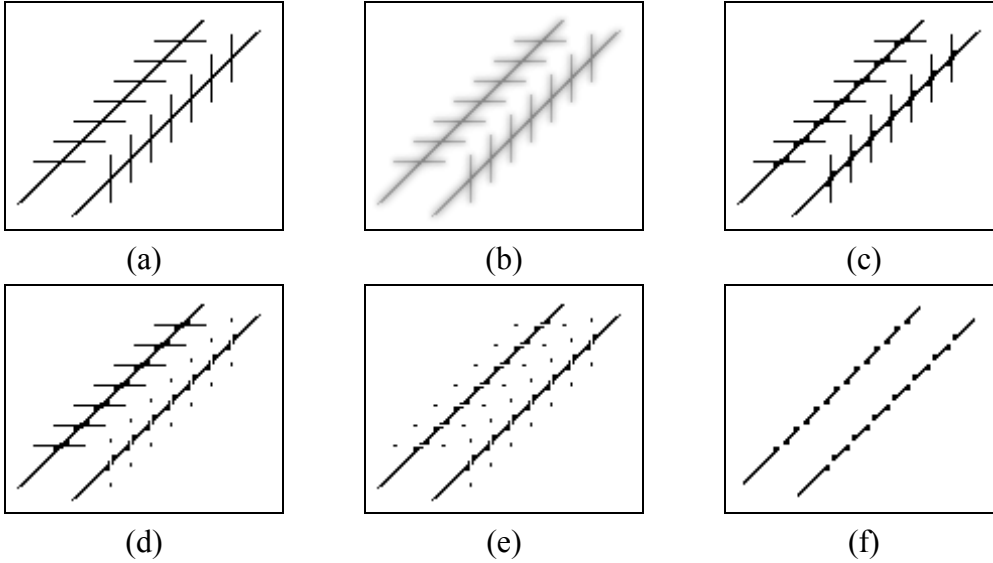


Figure 12. The original test image (a). The blurred image (b). The result of the threshold function (c). Erasing the vertical crossing lines (d). Erasing the horizontal crossing lines (e). The line pieces with the patches (f).

The result of this template is a gray-scale image. To get a black-and-white image again, we used this threshold template.

$$A=[2], \quad B=[0], \quad I=0.3 \quad (8)$$

(The initial state can be seen in Figure 12b, the output in Figure 12c.) The following three templates erase the crossing lines: (ha itt vagni akarsz akkor talan eleg az, ha azt mondom, hogy az orientacio erzekeny sejteken egy megvaltozott amplitudoeloszlast okoz ami elvezet az illuziohoz.)

$$A=[2], \quad B=[-0.2 \quad -0.2 \quad -0.2 \quad 1 \quad -0.2 \quad -0.2 \quad -0.2]^T, \quad I=-1.3 \quad (9)$$

(The input and the initial state are shown in Figure 12c, the output in Figure 12d.)

$$A=[2], \quad B=[-0.2 \quad -0.2 \quad -0.2 \quad 1 \quad -0.2 \quad -0.2 \quad -0.2], \quad I=-1.3 \quad (10)$$

(The input and the initial state are shown Figure 12d, the output in Figure 12e.)

$$A = \begin{bmatrix} 0 & 1 & 0 \\ 1 & 2 & 1 \\ 0 & 1 & 0 \end{bmatrix}, \quad B = [0], \quad I = 0 \quad (11)$$

(The initial state is shown Figure 12e, the output in Figure 12f.) For computing the orientation, there are orientation selective cells in the cortex [11]. The receptive field organization of the cells can be seen in Figure 13. Here we model a vertically oriented, orientation selective cortical cell type with the following template:

$$A = [0], B = \begin{bmatrix} -0.095 & -0.048 & 0.071 & 0.14 & 0.071 & -0.048 & -0.095 \\ -0.095 & -0.048 & 0.071 & 0.14 & 0.071 & -0.048 & -0.095 \\ -0.095 & -0.048 & 0.071 & 0.14 & 0.071 & -0.048 & -0.095 \\ -0.095 & -0.048 & 0.071 & 0.14 & 0.071 & -0.048 & -0.095 \\ -0.095 & -0.048 & 0.071 & 0.14 & 0.071 & -0.048 & -0.095 \\ -0.095 & -0.048 & 0.071 & 0.14 & 0.071 & -0.048 & -0.095 \\ -0.095 & -0.048 & 0.071 & 0.14 & 0.071 & -0.048 & -0.095 \end{bmatrix}, I = 0 \quad (12)$$

The inputs can be seen in Figure 14. The orientation of the line piece in the receptive field of a cell determines the output value of it. We tested the modeled orientation selective cell with three different images (Figure 14). Two of them were line pieces with patches at the ends (from Figure 12f), and the third was a same sized and oriented line piece without patches. This third one is considered as a reference image (Figure 14). The values of the responses are also indicated in Figure 14. According to the receptive field organization of the modeled cell type, the bigger the slope of the line in the receptive field, the greater the response is. Note that the responses are not proportional with the deviations. It is not surprising, because the way, how the cell computes the orientation is non-linear.

-	-	+	+	+	-	-
-	-	+	+	+	-	-
-	-	+	+	+	-	-
-	-	+	+	+	-	-
-	-	+	+	+	-	-
-	-	+	+	+	-	-
-	-	+	+	+	-	-

Figure 13. The receptive field organization of the modeled orientation selective cortical cell type.

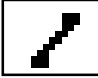
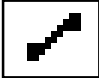
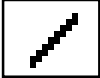
input image:			
cell response:	0.24	0.08	0.19

Figure 14. The images in the receptive field of the modeled orientation selective cells, and the response of them.

## 7.2 Brightness illusion

Figure 15a shows a basic brightness illusion. The two inner squares have the same brightness, but the outer different brightness of the frames cause us to judge them as different. This illusion

is a consequence of the lightness determination algorithm described in Section 5. The structure and templates was shown in Figure 8. If we put the original image (Figure 15a) to the sensory layer of the structure in Figure 8, we got a blurred image on the middle layer (Figure 15b), and got the final result (Figure 15c) on the third layer. It can be seen, that the inner squares on Figure 15c have truly different brightness, as the human observer really perceives it.

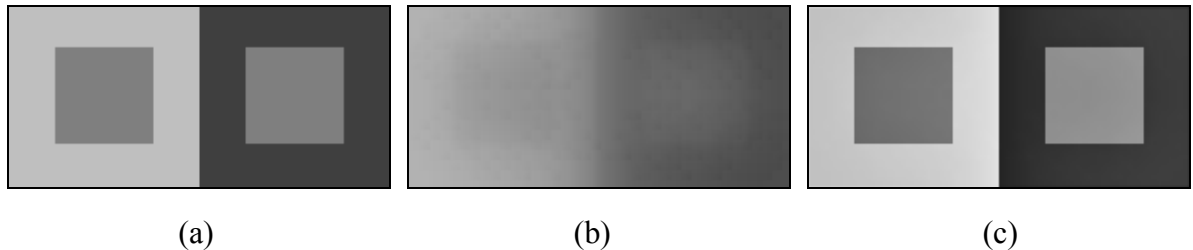


Figure 15. *The Brightness illusion. (a): the original image; (b) the blurred image; (c) the final result*

*(Talan ide rakhatnank ugyan ezekkel a templatekkel egy Mach band illuziot azt hiszem ide illik es mukodik is! Ha kell megcsinalom...).*

### 7.3 Cafe Wall illusion

In the vertebrate retinas the ganglion cells have center-surround antagonistic receptive fields. It means that the stimulation of the receptive field center of the neuron can be inhibited by the appropriate stimulation of the surround. This arrangement of the representation can explain the Cafe Wall illusion (Figure 16) [15]. On this illusion we can perceive convergence of the otherwise parallel edges of the tiles. The illusion strength depends on the thickness and brightness of the mortar and on the shift between the tiles.



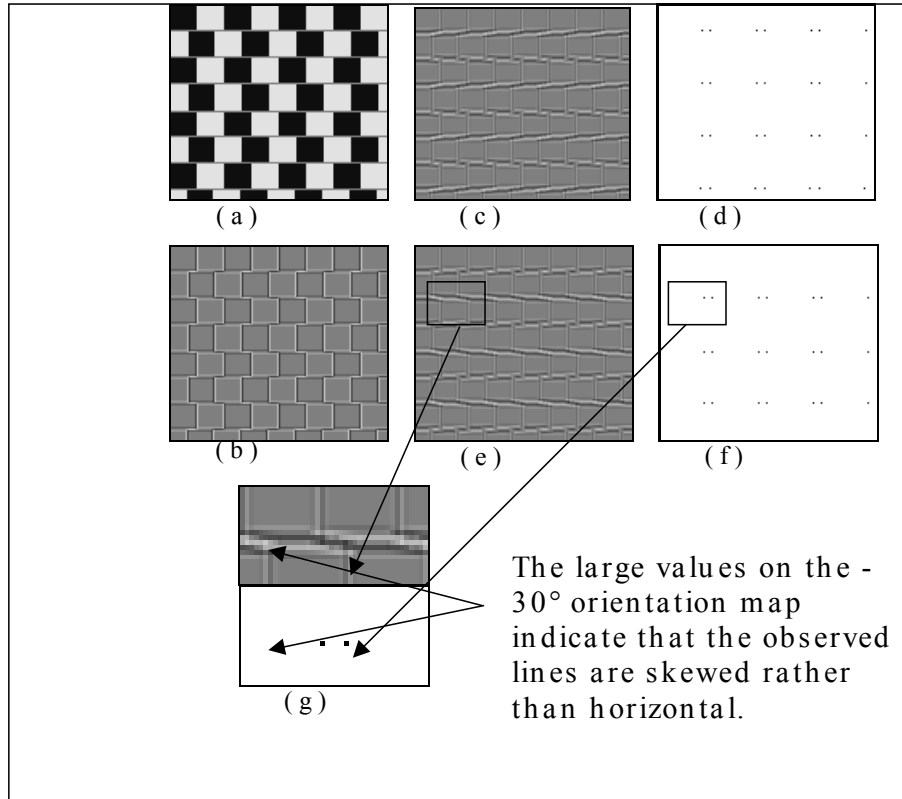


Figure 16. The Cafe Wall illusion (a) is explained by a center-surround filtering (b). The appearing tilt effect is exaggerated by +30° and -30° orientation filters (c, e). By thresholding these outputs we demonstrate the perceived illusion. On the enlarged inserts (g) the largest values indicates the existence of skewed lines in the particular positions. (d) and (f) demonstrate that different orientations observed in different positions according to the observed illusion.

If we use the next simple template:

$$B_{11} = \begin{bmatrix} -0.1 & -0.1 & -0.1 \\ -0.1 & 0.8 & -0.1 \\ -0.1 & -0.1 & -0.1 \end{bmatrix} \quad (13)$$

we can generate a representation (Figure 16b) of the visual stimulus (input image), which show some orientation tilt in that particular direction the illusion can be perceived. The template size and the applied template values were chosen for the simplest but good representation of the phenomenon and were robust in a wide parameter range. For the further exaggeration of this tilt effect we used +30° and -30° orientation filters and an appropriate threshold, which assumed to be present in the mammalian cortex as well. The used CNN templates were the followings:

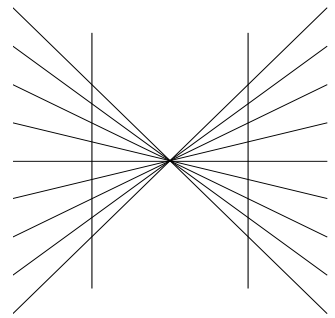
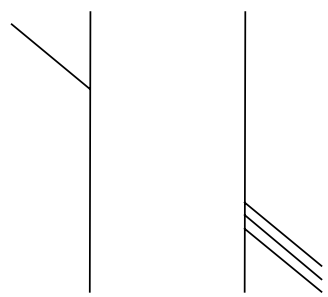
$$A_{12} = \begin{pmatrix} -0.1 & -0.1 & -0.1 & -0.1 & -0.2 \\ -0.1 & -0.1 & -0.1 & 0.2 & 0.2 \\ 0.2 & 0.2 & 0.2 & 0.2 & 0.2 \\ 0.2 & 0.2 & -0.1 & -0.1 & -0.1 \\ -0.2 & -0.1 & -0.1 & -0.1 & -0.1 \end{pmatrix} \quad A_{14} = \begin{pmatrix} -0.2 & -0.1 & -0.1 & -0.1 & -0.1 \\ 0.2 & 0.2 & -0.1 & -0.1 & -0.1 \\ 0.2 & 0.2 & 0.2 & 0.2 & 0.2 \\ -0.1 & -0.1 & -0.1 & 0.2 & 0.2 \\ -0.1 & -0.1 & -0.1 & -0.1 & -0.2 \end{pmatrix} \quad (14)$$

$$A_{23} = \begin{cases} 1 & \text{if } y \geq 0.48 \\ -1 & \text{if } y < 0.48 \end{cases} \quad A_{45} = \begin{cases} 1 & \text{if } y \geq 0.48 \\ -1 & \text{if } y < 0.48 \end{cases} \quad (15)$$

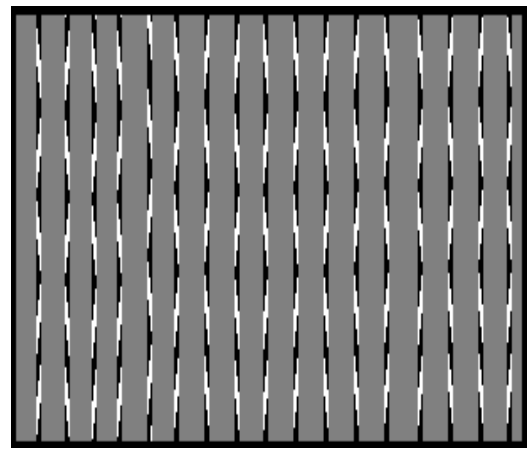
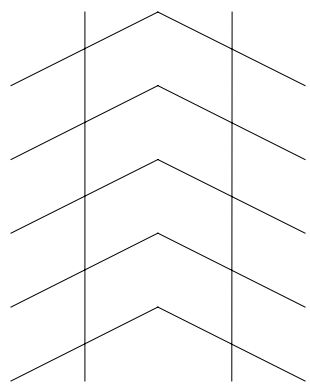
The achieved results of the CNN model can be seen on Figure 16.

#### 7.4 *Distortion illusions*

The Poggendorff illusion (Figure 17a,) is an old and still not totally understood illusion [15]. It has close relationship to the Zöllner, the Herring and the Twisted cord illusions (Figure 17b,c,d). There can be seen perceptual displacement of the oblique line in it. In the case of the Zöllner and Herring illusion one can observe deformation and divergence of the otherwise parallel lines. The twisted cord illusion pretends that the parallel cords are not straight as they really are. These illusions belong to the group of distortion illusions. There are several theories, which try to explain the underlying mechanisms of these illusions. We gave a reasonable model of Zöllner illusion earlier(!!!) in this paper. One supposed that common mechanisms are the exaggeration of the acute angles and minimization of the obtuse angles within the image. It is assumed, that the cortical lateral inhibition can produce corresponding effects [15]. That is, every orientation column is inhibiting the neighboring columns within the cortex and these interacting neighbors has usually resembling orientation preferences.



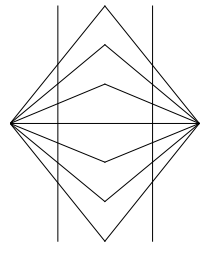
(a) (b)



(c)

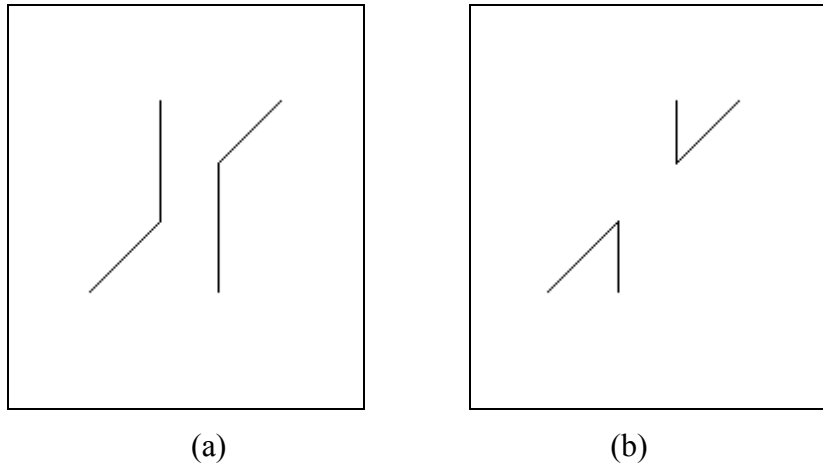
(d)

Figure 17. Different illusions, which can be explained by angular displacement theory. The Poggendorff (a), Herring (b), Zöllner (c) and the Twisted cord illusions (d).



(ez itt a Wundt, de lehetunk udvariasak is mert igen igen hasonlit a Herringre. Lehet hogy azt is annak nevezik, Nem hinnem hogy a kep kene, de megemlithetjuk mint hasonlot...)

However, in the case of Poggendorff illusion, there is considerable deviation from this rule, if we use a slightly different experimental condition. If we depict only the obtuse angles then we can still observe the illusion (Figure 18a). But in that situation, when only the acute angles are delineated exceptionally, the perceived illusion declines or even seems to disappear (Figure 18b).



*Figure 18. Special variants of the Poggendorff illusion. The illusion can be still perceived if all acute angles are erased (a), but decreases or disappears if the obtuse angles are eliminated (b).*

We can not find such a strange behavior in case of the other mentioned illusions. How can be explained this deviation from the otherwise suitable explanation? We presumed, that there has to be another phenomenon which can deteriorate the otherwise existing acute angle expansion. This can be the apparent, illusory shift of the position of the acute angles. If there exists such a phenomenon within the human visual information processing, then the other mentioned types of illusions will not be sensitive for this kind of shifts. On Figure 19 we demonstrate that there exists such a phenomenon. We can perceive that the tip positions alter depending on the acuteness of the different angles.

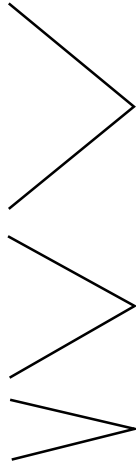


Figure 19. This image demonstrates, that one can perceive illusory shift in the tip position of different angles.

What type of mechanism causes the illusory shift of the acute angle's position, but does not change considerably the position of the obtuse angles and intersecting lines? If we use the next simple CNN template:

$$B_{11} = \begin{vmatrix} -1 & -1 & -1 \\ 0.5 & 0.5 & 0.5 \\ -1 & -1 & -1 \end{vmatrix} \quad A_{12} = \begin{matrix} 1 & \text{if } y \geq 0.3 \\ 0 & \text{if } y < 0.3 \end{matrix} \quad B_{12} = -1 \quad (16)$$

which is an orientation endpoint filter, we can detect the endpoints of the horizontal lines (Figure 20 b1). Apparently there is a slight overestimation or shift at the end position in case of acute angles (Figure 20 b2), but there is no identified endpoints neither at obtuse angles nor on the composite angle figures (Figure 20 b1, b3).

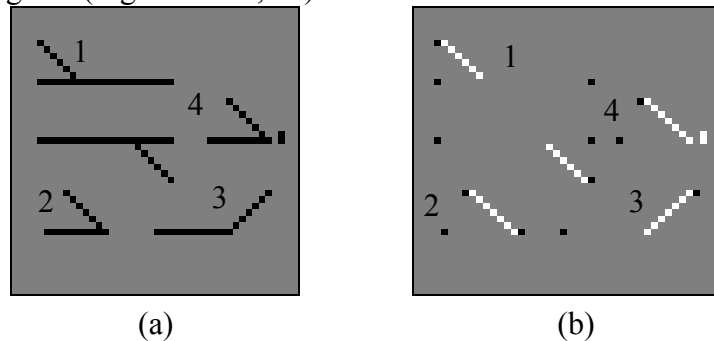


Figure 20. The CNN model of a special horizontal endpoint detection. The input can be seen on (a) and the result on (b) inserts. It can detect the endpoints of the acute angles (2) but it is not able to detect the obtuse angles (3) and the cross sections (1). By a distracting element (a(4)) this detector can be deceived (b(4)).

This way a simple orientation-endpoint filter can corrupt the effects of angle extensions. For validation of the existence of such a mechanism we changed slightly the experimental conditions.

We draw additional points nearby to the acute angles. This modification distract horizontal endpoint detector (Figure 20, b4), therefore the deterioration decrease and the Poggendorff illusion hopefully appears again. On (Figure 21,) we can compare the effects of the modified and the original stimuli.

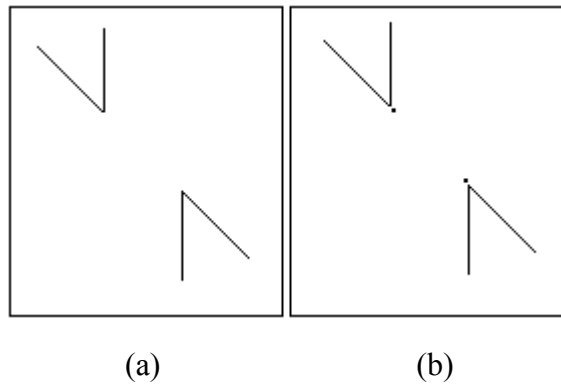


Figure 21. The effects of distracting elements on the strength of the Poggendorff illusion. There can be perceive a small displacement increase between parallel lines (b) compared observable to (a).

This suggested extension of the angular displacement theory can give explanation for the majority of the variations Poggendorff illusions. However, further scrutinized psychological experiments are necessary to verify our proposed explanation of this problem.

### 7.5 Face-vase illusion

Figure 22a shows the face-vase illusion. If the initial fixation point is inside the contour, we see a vase, otherwise we see two faces.

If we cannot decide exactly at once on an ambiguous scene which is the object, and which is the background, our brain will suppose that the fixation point is on the object. This happens here, if we look first at inside the vase, we will see a vase, and when we look first at one of the face, we will see the faces.

Our phenomenological model for this illusion contains a single layer CNN, having the following propagation type template:

$$A = \begin{bmatrix} 0 & 1 & 0 \\ 1 & 2 & 1 \\ 0 & 1 & 0 \end{bmatrix}, \quad B = \begin{bmatrix} 0 & 0 & 0 \\ 0 & -5 & 0 \\ 0 & 0 & 0 \end{bmatrix}, \quad I = 0 \quad (17)$$

If we consider our initial fixation point as a black spot in the initial state of the CNN, and put the original image (Figure 22a) to the input, the face or the vase will be extracted on the output of the CNN respectively. Figure 22 shows the effect.

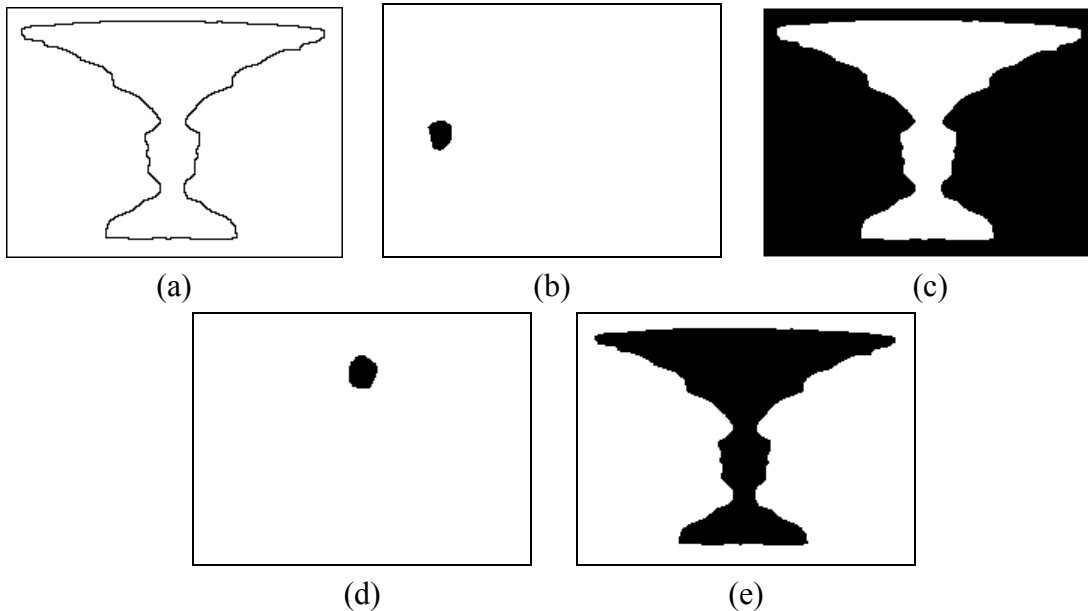


Figure 22. The face-vase illusion. (a): original image; (b) the fixation point is in the face area, (c) and the output of the CNN (c). The vase is extracted. If the initial fixation point is in the vase area (d), the vase is extracted (e).

## 7.6 Sculpture illusion1

The sculpture illusion (Salvador Dali's painting) can be seen in Figure 23a. After watching the image for a while, Voltaire's sculpture will suddenly appear.

There is a hidden sculpture in the center of the image, which can be considered as background at the first quick look (Figure 23a). It has the same grayness than the other background objects in that area. After watching the image for a while, our brain will segment the image by grayness, and analyze the shape and the structure of the groups of patches having the same gray level. In this way after a while, our brain will reconstruct and recognize Voltaire's sculpture.

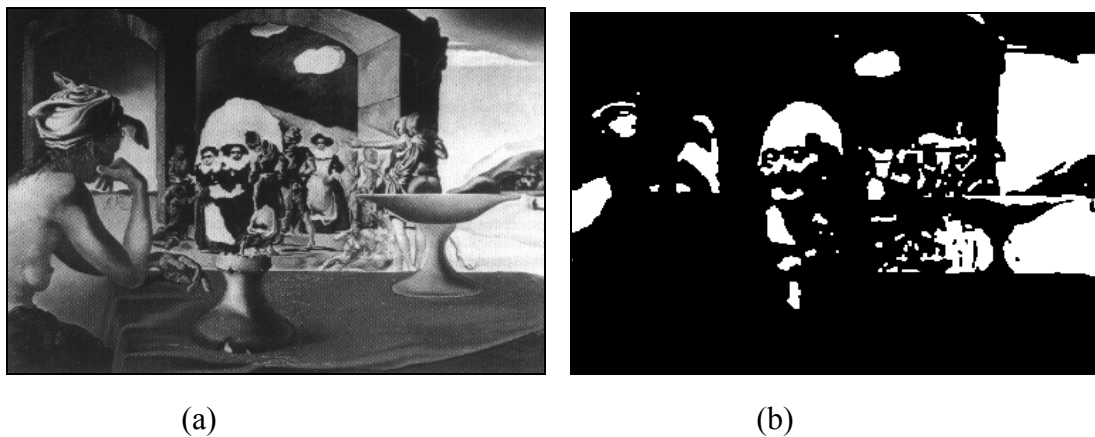


Figure 23. The sculpture illusion. The original input image (a), and the result (b).

We made a phenomenological CNN model for this illusion. The model contains a single layer CNN which segments the image by grayness by using the following CNN template:

$$A = \begin{vmatrix} 0 & 0.5 & 0 \\ 0.5 & 4 & 0.5 \\ 0 & 0.5 & 0 \end{vmatrix}, \quad B = \begin{bmatrix} 0.5 & 0.5 & 0.5 \\ 0.5 & 1 & 0.5 \\ 0.5 & 0.5 & 0.5 \end{bmatrix}, \quad I = 3.5 \quad (18)$$

The input and the initial state can be seen in Figure 23a and the output of the CNN is in Figure 23b. In the output image, the sculpture is obviously visible.

## 8. Conclusion

Different types of visual pathway CNN models were introduced in this paper. Some of them modeled the human color perception, others explained the appearance of the visual illusions.

## 9. Acknowledgment

The help of Professor Leon O. Chua and Professor Tamás Roska, and the supports of the *Hungarian State Eötvös Fellowship* and the grant *INT 90-01336* of the National Science Foundation in cooperation with the Hungarian Academy of Sciences, are greatly acknowledged.

## 10. References

- [1] E.H. Land, "Recent advantages in retinex theory and some implications for cortical computations: Color vision and the natural image", Proc. Natl. Acad. Sci. USA Vol. 80, pp. 5163-5169, August, 1983, Physics
- [2] E.H. Land, "The Retinex Theory of Vision", Scientific American, pp. 122-132, June 1978
- [3] B.K.P. Horn "Determining Lightness from an Image" Computer Graphics and Image Processing, 1974-3, pp.277-299, 1974.
- [4] L.O. Chua and L. Yang, "Cellular Neural Networks: Theory and Application", *IEEE Transactions on Circuits and Systems*, vol. 35, no. 10, October 1988, pp. 1257-1290
- [5] L.O. Chua and T. Roska, "The CNN Paradigm", *IEEE Transactions on Circuits and Systems - I*, vol. 40, no. 3, March 1993, pp. 147-156
- [6] T. Roska and L.O. Chua, "The CNN Universal Machine: An Analogic Array Computer", *IEEE Transactions on Circuits and Systems - II*, vol. 40, March 1993, pp. 163-173
- [7] T. Roska, J. Hámori, E. Lábos, K. Lotz, L. Orzó, J. Takács, P. L. Venetianer, Z. Vidnyánszky, Á. Zarándy "The Use of CNN Models in the Subcortical Visual Pathway", *IEEE Trans. Circuits and Systems* pp. 182-195, vol. 40, March 1993.
- [8] T. Roska, Á. Zarándy, L.O. Chua "Color image processing using multi-layer CNN structure" H Didiev(ed), *CircuitTheory and Design 93*, Elsevier, Amsterdam, 1993.



- [9] F. Werblin, T. Roska, and L.O. Chua, "The Analogic Cellular Neural Network as a Bionic Eye" *International Journal of Circuit Theory and Applications*, vol. 23, 541-569 (1995)
- [10] Á. Zarándy, T. Yang, T. Roska, and L.O. Chua, "CNN Based Models for Visual Illusions", 1995 International Symposium on Nonlinear Theory and Its Applications (NOLTA'95) pp. 471-476, Las Vegas, USA, Dec 10-14, 1995.
- [11] E.M. Kandel, J.H. Schwartz, "Principles of Neural Science", second edition, Elsevier New York, Amsterdam, Oxford, 1985.
- [12] F.Werblin, A.Jacobs, "Using CNN to Unravel Space-Time Processing in the Vertebrate Retina", *Proc. of the third IEEE Int. Workshop on Cellular Neural Networks and their Application (CNNA-94)*, pp. 33-40, Rome Dec. 1994.
- [13] K.Lotz, Z.Vidnyánszky, T.Roska, J.Vandewalle, J.Hámori, A.Jacobs, F.Werblin "Some Cortical Spiking Neuron Models Using CNN", *Proc. of the third IEEE Int. Workshop on Cellular Neural Networks and their Application (CNNA-94)*, pp. 41-46, Rome Dec. 1994.
- [14] A.Jacobs, T.Roska, F.Werblin "Techniques for constructing physiologically motivated neuromorphic models in CNN", *Proc. of the third IEEE Int. Workshop on Cellular Neural Networks and their Application (CNNA-94)*, pp. 53-60, Rome Dec. 1994.
- [15] S.Coren and J.S.Girgus, "Seeing is deceiving: The psychology of visual illusions", Lawrence Erlbaum Associates, Inc., New Jersey: 1978.
- [16] [HTTP://www.illusionworks.com](http://www.illusionworks.com)
- [17] E. Greene, "Both tilt and misalignment are manifestations of angular induction", *Percept. Mot. Skills* Vol. 73, pp. 329-330, 1993
- [18] E. Greene, D. Levison, "Angular induction as a function of the length and position of segments and gaps", *Perception*. Vol. 23(7), pp. 785-821, 1994
- [19] R.H. Day, E.J. Stecher, A.C. Parker, "The Poggendorff illusion and apparent interparallel extents", *Perception* Vol. 21(5), pp. 599-610, 1992